WILEY-VCH

Unrevealing temporal mechanoluminescence behaviors at high frequency via piezoelectric actuation

Tianhong Zhou, Haisheng Chen, Jiaxing Guo, Yanan Zhao, Xiaona Du, Qingyi Zhang, Wenwen Chen, Taiyu Bian, Zhi Zhang, Jiaying Shen, Weiwei Liu, Yang Zhang, Zhenping Wu,* Jianhua Hao**

T. Zhou, H. Chen, J. Guo, Y. Zhao, W. Chen, T. Bian, Z. Zhang, Prof. W. Liu, Prof. Y. Zhang
Institute of Modern Optics & Tianjin Key Laboratory of Micro-Scale Optical Information Science and Technology, Nankai University, Tianjin 300071, China
E-mail: yangzhang@nankai.edu.cn

X. Du
Institute of Photoelectric Thin Film Devices and Technology, College of Electronic Information and Optical Engineering, Nankai University, Tianjin 300350, China

Q. Zhang, J. Shen, Prof. Z. Wu
State Key Laboratory of Information Photonics and Optical Communications & School of Science, Beijing University of Posts and Telecommunications, Beijing 100876, China
E-mail: zhenpingwu@bupt.edu.cn

Prof. J. Hao
Department of Applied Physics, The Hong Kong Polytechnic University, Hung Hom, Hong Kong, P. R. China
E-mail: jh.hao@polyu.edu.hk.

Keywords: (mechanoluminescence, piezoelectricity, self-recovery, tunable luminescence, cluster)

Mechanoluminescence (ML) materials present widespread applications. Empirically, modulation for a given ML material is achieved by application of programmed mechanical actuation with different amplitude, repetition velocity and frequency. However, to date modulation on the ML is very limited within several to a few hundred hertz low-frequency actuation range, due to the paucity of high-frequency mechanical excitation apparatus. The

universality of temporal behavior and frequency response is an important aspect of ML phenomena, and serves as the impetus for much of its applications. Here, we push the study on ML into high-frequency range (~ 250 kHz) by combining with piezoelectric actuators. Two representative ML ZnS:Mn and ZnS:Cu, Al phosphors were chosen as the research objects. Time-resolved ML of ZnS:Mn and ZnS:Cu, Al shows unrevealed frequency-dependent saturation and quenching, which is associated with the dynamic processes of traps. From the point of applications, this study sets the cut-off frequency for ML sensing. Moreover, by *in-situ* tuning the strain frequency, ZnS:Mn exhibits reversible frequency-induced broad red-shift into near-infrared range. These findings offer keen insight into the photophysics nature of ML and also broaden the physical modulation of ML by locally adjusting the excitation frequency.

1. Introduction

Mechanoluminescence (ML) refers to the light emission in response to mechanical stimuli, such as stretching, compressing, impacting, grinding, and cleaving, etc. Depending on the choice of applied mechanical stimulus, ML can be divided into several categories, including fractoluminescence, triboluminescence, plasticoluminescence, and elasticoluminescence (EML)[1]. Among them, EML materials are capable of emitting reproducible luminescence through elastic deformation, and become the most investigated ML systems that promise extensive applications, such as stress sensing, structure crack monitoring, noncontact diagnosis, artificial skin and wearable devices[2]. To date, dozens of EML materials have been synthesized and developed. Multicolor ML has been realized by incorporating various lanthanide ions into host crystals, covering full spectrum from violet to near-infrared range[3]. Much endeavor has been devoted to finding efficient host systems including wurtzite CaZnOS[4, 5], perovskite compound $LiNbO_3$[6], and stuffed tridymite-type compounds $BaAl_2O_4$[7], etc. In addition to homogenous compounds, a series of heterostructures based on

ZnS/CaZnOS exhibit tunable and efficient EML process via band offsets at the heterojunction interface[8]. EML materials build a certain quantitative relationship between the mechanical stress and ML intensity in an *in situ* and real-time manner[9]. More intriguingly, EML can lead to self-powered devices without electric circuitry. This seamless and sustainable mechano-optical transduction gives rise to miscellaneous functionalities[10, 11]. Besides visualization of stress distribution, EML particles incorporated into translucent polymer can contact conformally with human body, and work as visualized sensing components for artificial skin and wearable devices[12, 13, 14]. The remote feature of EML-based sensing is expected to provide ultrasound-mediated noninvasive optical diagnosis and optogenetics[15, 16]. A notable concept of magnetic-induced luminescence (MIL) is established by strain-mediated coupling magnetic field with EML[17], realizing temporal and remote tuning of luminescence and color gamut via modulating magnetic field[18].

Despite some progress, ML phenomena are still not fully understood. Compared with well-known photoluminescence (PL) and electroluminescence (EL), the mechanisms behind diverse EML materials are still under controversy. A majority of EML materials are composed of piezoelectric hosts incorporating dopant lanthanide or transition metal ions, thus, piezoelectricity-induced carrier detrapping model is the most accepted explanation of EML to date[19, 20]. Besides the detrapping model, some groups claim that the triboelectric effect is also responsible for some EML (*e.g.* ZnS:Cu)[21, 22]. Ideal EML phosphors should generate sufficient bright and recoverable luminescence. The latter feature means the repeatability of ML under consecutive and repetitive mechanical stimuli without significant decay, which is an essential prerequisite for real applications. Up to now, most reported recoverable EML phosphors can recover to its initial intensity after UV light irradiation, which makes some post-processing indispensable[23]. Reproducibility of EML after light irradiation can be explained by retrapping carriers by exhausted traps, like a recharging process. Overall, EML can be regarded as a complex dynamic system with multibody interactions upon mechanical

activation, including energy bandgap, defect states, carriers, and dopant activators. But the photophysics of EML is much less understood, especially the dynamic processes of traps. To date, studies on EML-based materials and devices for both passive sensing and active emitting purposes are limited in the low-frequency stimulation. Frequency herein means the number of occurrences of a repeating mechanical stimulus per unit of time. Studying on dynamics of EML requires suitable excitation frequency, which is in some way analogous to kinetic description of photoluminescence processes requiring pulse width/frequency suitable laser source. Unlike dazzling choices of pulsed lasers, available mechanical excitation apparatus, especially high-frequency source, is very limited[24]. Mechanical test machine and weight drop tower can apply load stress in a few hertz (Hz). The operating frequency of mechanical stretching-releasing systems is generally limited in several hundred hertz. Considering the trapping and detrapping times of semiconductor defects ranging from a few microseconds to hundreds of microseconds, mechanical excitation sources endowed with a frequency of tens of kilohertz (kHz) or even higher are fairly essential. Piezoelectric materials enable efficient electromechanical transduction. Actuators made of piezoelectrics offer the desired linear strain with fast actuation upon the drive voltage. Under the excitation of alternating current (AC) electric fields, piezoelectric actuators can produce instantaneous mechanical deformation up to megahertz (MHz) range. Thus, piezoelectric actuator as an idea platform provides access to fundamental elements related to EML, including the dynamics of traps, the motion of carriers, as well as the deactivation and energy transfer of activated ions. In this work, we investigate the temporal response characteristics of EML based on piezoelectric actuator made of $Pb(Mg_{1/3}Nb_{2/3})O_3$-$PbTiO_3$ (PMN-PT). Considering both the universality and adaptability of this study, the most classic and common EML compounds doped ZnS (e.g., ZnS:Mn and ZnS:Cu, Al) were chosen as the research objects. Previous studies have shown that ZnS:Mn and ZnS:Cu, Al possess high luminescent intensity and reproducibility (Supplementary **Fig. S1**)[25], making them the best candidates for in-depth

investigation and hypothesizing the EML dynamics and underlying mechanisms. Herein, we present the first demonstration of EML responses upon high-frequency stimulation. Time-resolved ML of ZnS:Mn and ZnS:Cu, Al shows unreported frequency-dependent saturation and quenching, which is determined by the dynamic processes of traps. From the point of applications, this study sets the cut-off frequency for EML sensing applications. Moreover, ZnS:Mn exhibits unrevealed frequency-induced broadband red-shift to NIR region. These findings offer opportunities to gain new insight into the nature of ML in frequency domain.

2. Results and Discussion

Frequency response of ZnS:Mn. **Figure 1a** shows the schematic setup for steady state and transient state EML measurements (see Methods). **Figure 1b** depicts the hybrid structure of the adjacent UV adhesive layer embedded with ZnS:Mn particles integrated with PMN-PT substrate. UV curable adhesive was chosen as the matrix material for the dispersed ZnS:Mn phosphor. The UV-curing approach allows the phosphor laminate to be densified and tightly adhered to gold-covered PMN-PT surface at room temperature with simple UV radiation. ZnS:Mn microparticles were mixed into the UV adhesive. The EML composite layer used in the experiment was set to a thickness of 200 μm for maintaining the uniformity of the laminate layer. The scanning electron microscopy (SEM) image shows the microstructure of the resultant composite (Supplementary **Figure S2**). Supplementary **Figure S3** shows the X-ray diffraction (XRD) patterns of ZnS:Mn and ZnS:Cu, Al powders, confirming the wurtzite structure (JCPDS No. 36-1450) of the powders. X-ray photoelectron spectroscopy (XPS) result in **Figure S4** shows that the binding energies of Mn $2p_{3/2}$ and Mn $2p_{1/2}$ locate at 641.5 and 653.1 eV, respectively, confirming the Mn^{2+} valence state in the ZnS:Mn composite. The EML features of ZnS:Mn composite are firstly investigated by applying rectangular wave voltage of different amplitudes on PMN-PT at fixed frequency (200 Hz). **Figure 1c** shows the EML intensity as a function of the amplitude of the applied voltage V_0 increasing from 181 to

261 V. To ensure no damage to the device, the experimental voltage applied in the test condition is less than the critical voltages, so that the integrity of the substrate can be guaranteed during the measurement. The PL emission of the sample under the excitation of 365 nm is also investigated (Supplementary **Figure S5**). In PL spectrum, the weak emission around 475 nm is associated with the self-activated defect sites induced by the zinc vacancy (V_{zn}). The intense emission at 593 nm results from the $^4T_1 \rightarrow {}^6A_1$ transition of Mn^{2+} ion. The orange emission bands at 593 nm in all EML spectra also result from the $^4T_1 \rightarrow {}^6A_1$ transition of Mn^{2+} ion, which is similar to previously reported EML results of ZnS:Mn. As shown in Supplementary **Figure S6**, the EML intensity almost maintain a linearity with increasing V_0^2, which is consistent with the proposed model[25]. With further increasing frequency, the observed ML intensities deviate from the theoretical model in Ref. 25, and present unrevealed frequency-dependent saturation and quenching. As shown in **Figure 1d**, the EML intensity increases along with the increment of excitation frequency. EML intensity around 593 nm reaches its peak at 4 kHz. Moreover, an extra broad band ranging from 635 nm to 930 nm can be observed when the frequency reaches 4 kHz. As the excitation frequency increases from 100 Hz to 100 kHz, the temperature of the ZnS:Mn composite increases from 25.8 ºC to 26.2 ºC. The tiny temperature increment cannot result in such broad redshift of EML spectrum (Supplementary **Figure S7**). In a controlled experiment, pure ZnS composite was integrated with PMN-PT actuator. Upon piezoelectric strain, there is no EML emission observed in pure ZnS composite (Supplementary **Figure S8**), excluding the possibility of broad near-infrared (NIR) emission as a result of the defects inside ZnS. The broad emission spectrum can be decomposed into five Gaussian components centered at 636, 701, 772, 842 and 911 nm, respectively, which is attributed to the formation of $(Mn)_n$ clusters (n = 2-6)[26]. Further increasing the excitation frequency, it is interesting to find that the single Mn^{2+}-related emission (593 nm) is continuously suppressed, while NIR emissions from $(Mn)_n$ clusters

continue to increase and dominate the spectrum (**Figure 1e** and Supplementary **Figure S9**). Note that 30 kHz marks a turning point, NIR emission begins to decrease and is strongly quenched when the frequency increases to 200 kHz (**Figure 1f**), which will be discussed below.

Integrating EML laminate with piezoelectric actuator offers the opportunities to explore EML response upon high-frequency stimulation, where some intriguing phenomena happen. We have revealed that EML of ZnS:Mn undergoes three phases in response to the frequency, as shown in **Figure 2a** and **2b**. Under low-frequency excitation (≤ 200 Hz), EML emission of ZnS:Mn mainly originates from single Mn^{2+} ion and keeps a linear growth with the frequency, conforming to conventional perception. Further increasing the excitation frequency, EML intensity centered at 593 nm exhibits a nonlinear increment until reaching the saturation. At the same time, a distinguishable broad NIR emission band in the range of 635 to 930 nm came from the $(Mn)_n$ clusters (n = 2-6) begins to rise and dominate the emission profile. Increasing the excitation frequency contributes to such a contrary tendency of red and NIR emissions. Similar characteristics have been observed in Mn-concentration dependent PL and EL from ZnS:Mn. As already reported, ZnS:Mn with high Mn concentrations exhibit both orange emission band and NIR emission bands in both PL and EL measurements[27, 28]. In addition, the relative intensity ratio of the NIR to orange emission increases with increasing Mn concentration. It is believed that higher concentration of the Mn dopant contributes to the formation of $(Mn)_n$ clusters, resulting in the enhancement of the NIR emission. However, things are different in our case. The embedding of Mn^{2+} ions inside the ZnS lattice would give rise to Mn-Mn interaction, which can be verified by the electron paramagnetic resonance (EPR) spectra. Supplementary **Figure S10** shows the EPR spectrum of the ZnS:Mn composite. Typical six hyperfine lines appear for ZnS:Mn with lower Mn concentration. In our case, the measured EPR spectrum contains both hyperfine structures as well as a broad

resonance line, confirming the formation of $(Mn)_n$ clusters[29]. But, both PL and low-frequency EML results indicate only small amount of the $(Mn)_n$ clusters existing in the ZnS:Mn composite. As shown in **Figure 1d** and Supplementary **Figure S4**, both low-frequency excited EML and PL from ZnS:Mn composite only find the orange emission band, negligible NIR emission can be observed. The emergence of NIR emission and its enhancement along with the quenching of the orange emission, only happen upon higher frequency excitation (> 2 kHz). Previous studies on ZnS:Mn have found that the excitation energy is not localized at a particular Mn atom, and rather migrates between nearest-neighbour and next-nearest-neighbour Mn-pairs. When repetitive rectangular wave voltages are applied on the piezoelectric PMN-PT, the PMN-PT substrate can impose in-plane compressing-releasing strain on ZnS:Mn laminate at the same waveform of the voltage. Such a modulation will induce the change of the distances between Mn^{2+} ions and other NIR emission centers. Coupled $(Mn)_n$ clusters will be formed when Mn^{2+} ions become close enough[30]. The increment of the excitation frequency increases the probability of the formation of $(Mn)_n$ clusters. Furthermore, it facilitates the energy transfer from excited Mn^{2+} ions to the $(Mn)_n$ clusters, which leads to the appearance and enhancement of NIR emission band[31].

Besides the additional emission band in the NIR region, high-frequency stimulation also contributes to EML quenching, which hasn't been reported so far. Our device unravels the frequency response characteristics of orange and NIR emissions from ZnS:Mn. Orange emission reaches its peak at 4 kHz, and is almost disappeared at 9 kHz (**Figure 2a**). While, NIR emission arrives at the peak around 30 kHz, and further increasing frequency leads to EML quenching (**Figure 2b**). Schematic illustration of piezoelectricity-induced detrapping model for ZnS:Mn is shown in **Figure 2c**. The lattice of the PMN-PT substrate will change along the direction of the electric field. Such a modulation in the lattice parameter will cause changes in the in-plane lattice parameters as a result of the Poisson effect, which can

subsequently impose in-plane strains in the ZnS laminate. Upon strain, piezoelectric field can decrease the trap depth or tilt the band structure, resulting in the detrapping of electrons from filled-electron defect states to the conduction band. Following with excitation of Mn^{2+} ions via non-radiative energy transfer from electron-hole recombination, EML emission arises due to the de-excitation of excited Mn^{2+} ions. **Figure 2d** shows that NIR emission is attributed to the formation of $(Mn)_n$ clusters and energy transfer from an excited Mn^{2+} ion to $(Mn)_n$ clusters upon high-frequency excitation. To some extent, the proposed piezoelectricity-induced detrapping model is equivalent to a piezophotonic effect, *i.e.* a two-way coupling between piezoelectricity and photoexcitation processes[32]. According to the trap-related model, the EML dynamics involves piezoelectrically promoted detrapping and retrapping, non-radiative recombination and subsequent energy transfer processes. Considering the time required for the nonradiative recombination and energy transfer processes is much smaller than that of detrapping and retrapping electrons at shallow donor states, we deduce that frequency-related quenching EML of ZnS:Mn under high-frequency stimulation is associated with the detrapping and retrapping step: the release or capture rate cannot catch up the frequency of mechanical stimuli.

In order to verify the hypothesis, we investigate the time-resolved EML of ZnS:Mn under different frequency excitation. When subjected to cyclic rectangular wave strain, ZnS:Mn composite emits repeatable EML pulses. As shown in **Figure 3a-3c** and Supplementary **Figure S11**, once the excitation frequency is smaller than 20 kHz, two luminescent pulses can be observed upon one cycle of applied strain, which is consistent with previous reports. The first and secondary EML pulses correspond to the compressing and releasing strain, respectively. For the first EML pulse, instantaneous compressing strain promotes the detrapping of electrons and results in EML emission. Then the bias voltage keeps unchanged, the EML intensity gradually increases to the peak until exhaustion of the trapped electrons,

then decreases with time. The secondary EML pulse upon abrupt release of strain is maybe associated with the viscoelasticity of the ZnS:Mn composite or the triboelectricity-induced ML. Based on the Boltzmann superposition principle, the abrupt release of piezoelectric stress is equivalent to the sum of stress before releasing plus an equal amount stress in the negative direction. The consequent recovery strain in Supplementary **Figure S12** could give rise to the secondary EML pulse phenomena[33, 34]. Another possibility of the secondary EML pulse could arise from the triboelectricity-induced ML, rather than piezoelectricity-induced ML. A certain amount of charge accumulate at the interface between the ZnS:Mn particle and the matrix material during the shrink and retreat processes. The triboelectric field can trigger the observed luminescence processes. For analysis purposes, we introduce the rise and fall times. The rise time is defined as the time span from the moment of strain applied to the EML pulse reaches its maximum. And the fall time means the time required for the EML pulse decreases from the peak to the ground. We measured the rise and fall times for NIR emission versus the excitation frequency for analyzing the dynamic processes. As shown in **Figure 3d**, when the excitation frequency is below 12 kHz, the rise and fall times demonstrate relatively stable values around 9.7 μs and 35.1 μs, respectively. When the amplitude and changing rate of strain are given, the rise time strongly depends on the detrapping rate, and the fall time is determined by the decay time of luminescence of Mn^{2+} ions. Further increasing the frequency, the decay process would be interrupted by the strain releasing, no longer calculating the fall time in the frequency range above 12 kHz. In Supplementary **Figure S13**, the rise time maintains stable value (~ 9.7 μs) up to 30 kHz, confirming that the detrapping rate keeps stable until 30 kHz. If further increase the frequency, the rise times begin to decrease. The rise times corresponding to 40 kHz and 50 kHz are 7.2 μs and 5.8 μs, respectively. Suppose the detrapping rate keeps constant under the same strain, the decrease of rise time upon higher frequency excitation could arise from the reduction in the number of accumulated electrons during the retrap process. This explains why EML reaches its peak at about 30 kHz: at a

higher frequency, there is no enough time to complete the retrap process. In order to further distinguish the impact of detrapping and retrapping rate, the turning-point frequency is defined as the frequency of EML intensity reaching its maximum. **Figure 3e** shows the turning-point frequency as a function of applied voltage amplitude. It can be found that with increasing the applied voltage amplitude, the turning-point frequency shifts to lower frequency. According to previous analysis, upon the pressure P applied on the piezoelectric sample, the trap depth of electrons will decrease from E_0 to E_p[18]:

$$E_P = E_0 - \frac{2q^2\lambda^2 P\dot{P}t}{\kappa\epsilon^2} \quad (1)$$

where q is the electron charge, λ is the piezoelectric coefficient, $\dot{P} = dP/dt$ is the pressing rate on the sample, κ is the force constant of the host lattice, and ε is the permittivity. When E_p becomes comparable to kT (here k is the Boltzmann constant and T is the absolute temperature), the detrapping process occurs. The detrapping rate of electrons can be written as[19]:

$$-\frac{dn_t}{dt} = \frac{dn_t}{dE_P}\frac{dE_P}{dt} = \frac{2Zq^2\lambda^2 P\dot{P}n_t}{\kappa\epsilon^2} \quad (2)$$

where n_t is the number of trapped electrons, Z is the distribution coefficient of traps. From Equation (2), it is conceivable that higher applied voltage corresponds to larger pressing situation, resulting in larger detrapping rate. In principle, if high-frequency excitation-induced EML saturation is determined by the detrapping rate, larger detrapping rate would contribute to higher turning-point frequency, which is contrary to our observation. Thus, we can conclude that EML saturation and quenching of ZnS:Mn arise from the retrapping rate rather than detrapping rate lags behind the excitation frequency (**Figure 3f**).

ZnS:Cu, Al is another important self-recoverable EML material. In a parallel study, its frequency response characteristics were also investigated for validating and enriching our

perception of the frequency response of EML. Unlike ZnS:Mn, EML emissions from ZnS:Cu, Al arise from donor-acceptor recombination. Measurements were performed by applying rectangular wave voltages of varying amplitude and frequency on the similar device shown in **Figure 1a**. EML spectra of ZnS:Cu, Al composite versus the voltage amplitudes at fixed 100 Hz are shown in Supplementary **Figure S14**. Under low-frequency excitation, mainly green emission band centered at 525 nm can be found. This green emission is attributed to donor-acceptor pair recombination, in which Al^{3+} substitutes for Zn^{2+} (Al_{Zn}) at donor level, and Cu^{+} substitutes for Zn^{2+} (Cu_{Zn}) at acceptor level. Supplementary **Figure S15** shows that the green EML intensity is almost linear with increasing V_0^2, which is similar to ZnS:Mn results. **Figure 4a** and **4b** demonstrate the EML spectra of ZnS:Cu, Al composite under the excitation frequencies from 50 Hz to 140 kHz, the applied voltage was kept at 165 V. With increasing the frequency, a blue emission around 450 nm occurs, which is due to the recombination between sulphur vacancy (V_s) related donor and Cu_{Zn} related acceptor. **Figure 4c** and **4d** show the blue and green emission intensities as a function of excitation frequency, respectively. It can be found that both blue and green emission intensity enhance with increasing the frequency from 50 Hz to 48 kHz. Furthermore, it looks like the blue emission grows faster. Once the excitation frequency is over 3300 Hz, the blue emission component is over than the green band, and further dominates the spectra shape at 18 kHz. Further increasing the frequency over 48 kHz, both the blue and green emission bands reach their peaks, and begin to decrease with the increment of excitation frequency, which is similar to the frequency response characteristics of ZnS:Mn. **Figure 4e** depicts the schematic illustration detailing the EML mechanism of ZnS:Cu, Al. V_s and Al_{Zn} create shallow and deep donor states under conduction band, which act as trapping centers for electrons. While, Cu_{Zn} creates deep acceptor-like states and can catch holes from the valence band. Blue and green emissions in ZnS:Cu, Al have been interpreted as a result of electron-hole recombination of donor-acceptor V_s - Cu_{Zn} and Al_{Zn} - Cu_{Zn} pairs, respectively. The spectra profile changing in response to the

frequency can be elucidated by the trap-controlled donor-acceptor pair emission mechanism. Upon compressing strain, electrons detrap from both V_s and Al_{Zn} donor levels, and recombine with the holes in Cu_{Zn} acceptors, resulting in blue and green EML emissions. In principle, the optical transition probability of these two pair emissions is determined on the intra-pair separation[35]. Smaller intra-pair separation is in favor of a higher electron-hole recombination rate. **Figure 4f** shows the EML response of blue and green emissions. The decay time for blue and green emission are 15.2 μs and 31.6 μs, respectively, indicating the intra-pair distance between V_s - Cu_{Zn} is smaller than that of Al_{Zn} - Cu_{Zn} pair. Smaller intra-pair distance between V_s - Cu_{Zn} contributes to the increased overlapping of the pair's wavefunction. Thus, EML emission from V_s - Cu_{Zn} pairs is susceptible to saturation upon enhanced excitation. Therefore, with increasing excitation frequency, the blue emission gradually dominates the EML spectra. This explanation can be also verified by the PL spectra of ZnS:Cu, Al under different excitation power density. As shown in Supplementary **Figure S16**, with increasing excitation power density, the blue emission band also gradually surpasses the green emission, further confirming our hypothesis.

Figure 5a-5b and Supplementary **Figure S17** show the time-resolved EML of ZnS:Cu, Al by a cyclic compressing-releasing stress. Like ZnS:Mn, two luminescent pulses occur in response to the compressing and releasing strain, which can be attributed to the piezoelectric- and triboelectric-mediated ML mechanisms. It also can be found that with increasing the excitation frequency, the EML spectra become weak and irregular. **Figure 5c** shows that the rise time for blue emission keeps a stable value ~ 6.6 μs. However, the fall time for ZnS:Cu, Al exhibits a declining trend with increased frequency. This is because with increasing excitation frequency, the blue emission component gradually occupies the mainstream status. And the blue emission endows with a faster decay time as mentioned above. Turning-point frequency of ZnS:Cu, Al in **Figure 5d** tends to lower frequency when the applied voltage

increases, indicating the retrapping rate is also responsible for the EML saturation and quenching of ZnS:Cu, Al. The observed phenomena of ZnS:Cu, Al confirms our explanation on frequency response of trap-controlled EML.

The study on EML upon high-frequency stimulation is more than fundamental curiosity. The ability to manipulate color output of EML materials is important for their applications as light sources, displays, and multiplexed bioimaging. Moreover, NIR EML is highly desirable to visualize the inner biological stress because it can penetrate biological tissues. Here, we demonstrate that excitation frequency represents a novel powerful and convenient "tuning knob" for in situ and reversible color tunability. The calculated Commission Internationale de L'Eclairage (CIE) coordinates in **Figure 5e** suggest that the excitation frequency-tunable color emissions from ZnS:Mn and ZnS:Cu, Al covering red-green-blue three primary colors. Notably, self-recoverable NIR ML emission has been obtained thanks to the relatively broad frequency range provided by piezoelectric actuators. Regulating the mixing ratio of two or more EML phosphors promises more colorful displays. As a proof of concept, we achieve a series of letters with real-time tunable white and multicolor emissions as shown in **Figure 5f**. Excitation frequency represents an additional degree of freedom in the control of color gamut for EML phosphors.

3. Conclusion

It should be noted that EML materials and devices are self-powered, because they sense or harvest environmental mechanical energies without the need of batteries or electrical cables, and thereby promise more device design freedom. In the moderate strain range, the measured ML intensity of the trap-controlled EML materials is found to be proportional to the amplitude and changing rate of strain. There is no experimental evidence to support this empirical conclusion appropriate in high-frequency excitation range. It may encounter high-

frequency mechanical vibrations in the application of EML, such as high-frequency sound, ultrasonic wave, and vibration in bearings, etc. Moreover, temporal response is an intrinsic characteristic of a luminescent material. Time-resolved PL and EL have provided more insight into the species excited state dynamics and greatly benefited numerous application areas. However, temporal responses of EML have yet to be demonstrated, impeded by the lack of high-frequency mechanical sources. Herein, we present the first demonstration of EML characteristic upon high-frequency stimulation. ZnS:Mn exhibits unrevealed frequency-induced red-shift and quenching of EML with increasing excitation frequency. The emergence and enhancement of NIR emission, along with suppressing the original orange emission are due to the increment of the excitation frequency promoting the formation of $(Mn)_n$ clusters and energy transfer from excited Mn^{2+} ions to the $(Mn)_n$ clusters. It should be noted that with increasing the frequency to the high-frequency range, the observed ML intensities deviate from the empirical model, and present unrevealed frequency-dependent saturation and quenching. These results could set the cut-off frequency for sensing high-frequency mechanical signals. Time-resolved EML of ZnS:Mn reveals that frequency-dependent quenching is associated with the retrapping rate, which cannot catch up with excitation rate at a high-frequency range. While, ZnS:Cu, Al shows similar EML saturation and quenching upon high-frequency stimulation, further confirming our explanation on temporal response of EML. Moreover, the emission bands of ZnS:Cu, Al shift towards higher energy with increasing excitation frequency, which is interpreted by the trap-controlled donor-acceptor pair emission mechanism. In terms of methodology, the characterization of defect traps and their dynamics are highly challenging. Diverse techniques, such as deep-level transient spectroscopy, photoinduced current transient spectroscopy, and time-of-flight current spectroscopy have been developed. We have gained the trapping and detrapping information by analyzing the temporal ML behavior, which paves a new way for exploring dynamic information of traps. These results push the study on EML into previously

unexplored high-frequency range, and time-resolved EML response provides new insight and understanding of the trap-controlled mechanism. This study demonstrates temporal full-color tuning via modulating electric field aiming for constructing more compact and colorful EML light sources and displays.

4. Experimental Section

EML Composite and Device Fabrication: Metal-ion doped ZnS phosphors (ZnS:Mn and ZnS:Cu, Al purchased from Global Tungsten & Powders) were uniformly mixed into the UV-curable adhesive (Ausbond A332) matrix at a weight ratio of 3:7. Commercial 5 × 5 mm^2 (001)-oriented PMN-PT single crystals (Hefei Kejing Material Technology Co, Ltd.) was used as the piezoelectric substrate. Ti/Au (5 nm/40 nm) layer was thermally evaporated on the surface of PMN-PT as the electrode. The EML composite layer with the thickness of 200 μm was spin-coated on the gold-coated PMN-PT substrate and irradiated with UV lamp (365 nm) for 45 min for curing. The top and bottom electrodes were led out with silver paste and silver wire.

Characterizations and Luminescence Measurements: X-ray diffractometer (Bruker D8 Discover: λ = 1.5406 Å, Cu Kα1 radiation) was used to characterize the crystal structure of the samples. Figure S1 and S2 show the corresponding XRD patterns of ZnS:Mn and ZnS:Cu, Al, respectively. Scanning electron microscopy and energy-dispersive X-ray (EDS) spectroscopy analysis were investigated by a Zeiss Sigma 500 field emission SEM system. X-ray photoelectron spectroscopy (XPS) measurements were carried out using a ThermoFisher Scientific ESCALAB 250Xi instrument. Electron paramagnetic resonance (EPR) was performed using a Bruker EMX PLUS spectrometer at the frequency of 9.8 GHz at room temperature. Figure 1a shows the schematic of the setup for steady and transient state ML measurements. The photoluminescence (PL) and EML spectra of the samples were measured

with a SpectraPro 300i spectrophotometer. 355 nm laser diode was used as the excitation source. AC voltage was applied to PMN-PT substrate using a Rigor DG4202 signal generator connected to a HA820 voltage amplifier. PMN-PT substrate was polarized using a Keithley 2410 Source-Meter with a high-voltage output before applying the AC voltage. Time-resolved EML was recorded with a photomultiplier coupled with Tektronix DPO3034 oscilloscope. Infrared thermometer (DELIXI DECTMM520C) was used to measure the temperature of sample upon actuation. The infrared thermometer possesses 0.1 degree Celsius, and can provide immediate surface temperature with a non-contact manner. The luminescence photos were taken by a mirrorless camera (Sony NEX-5N) with a Sigma (56mm 1.4) lens.

Supporting Information

Supporting Information is available from the Wiley Online Library or from the author.

Acknowledgements

This work was supported by the National Natural Science Foundation of China (No. 11874230, 12074044, 12274243, 52233014), the Research Grants Council of Hong Kong (PolyU SRFS2122-5S02), the Fund of State Key Laboratory of Information Photonics and Optical Communications (IPOC2021ZT05), the Natural Science Foundation of Tianjin (18JCYBJC41500), and the Fundamental Research Funds for the Central Universities (BUPT).

Conflict of Interest

The authors declare no conflict of interest.

Author Contributions

Y.Z. conceived the experiment and supervised the project together with Z.W. and J. H. who direct the research. The devices were designed and fabricated by T.Z. and Y.Z., Optical experiments were performed by T.Z. and H.C. X.D. performed the SEM and XRD measurements. J.G., Q.Z. and W.C. contributed to the characterization of samples. J.S. and T.B. implemented the measurement setup. Z.Z. and W.L. conducted the photoresponse measurements. Y.Z., Z.W. and J.H. wrote the paper with contributions of all authors.

Received: ((will be filled in by the editorial staff))

Revised: ((will be filled in by the editorial staff))

Published online: ((will be filled in by the editorial staff))

References

1. Zhang J-C, Wang X, Marriott G, Xu C-N. Trap-Controlled Mechanoluminescent Materials. *Progress in Materials Science* **103**, 678-742 (2019).
2. Chen B, Zhang X, Wang F. Expanding the Toolbox of Inorganic Mechanoluminescence Materials. *Accounts of Materials Research* **2**, 364-373 (2021).
3. Du Y*, et al.* Mechanically Excited Multicolor Luminescence in Lanthanide Ions. *Advanced Materials* **31**, 1807062 (2019).
4. Tu D, Xu C-N, Fujio Y, Yoshida A. Mechanism of mMechanical Quenching and Mechanoluminescence in Phosphorescent CaZnOS:Cu. *Light: Science & Applications* **4**, e356-e356 (2015).
5. Zhang X*, et al.* Tuning Multimode Luminescence in Lanthanide(III) and Manganese(II) Co-Doped CaZnOS Crystals. *Advanced Optical Materials* **8**, 2000274 (2020).
6. Tu D, Xu C-N, Yoshida A, Fujihala M, Hirotsu J, Zheng X-G. $LiNbO_3:Pr^{3+}$: A Multipiezo Material with Simultaneous Piezoelectricity and Sensitive Piezoluminescence. *Advanced Materials* **29**, 1606914 (2017).

7. Rai RK, Upadhyay AK, Kher RS, Dhoble SJ, Mehta M. $BaAl_2O_4$:Eu – Phosphor for Mechanoluminescence Dosimetry. *Radiation Measurements* **46**, 1393-1396 (2011).

8. Peng D*, et al.* A ZnS/CaZnOS Heterojunction for Efficient Mechanical-to-Optical Energy Conversion by Conduction Band Offset. *Advanced Materials* **32**, 1907747 (2020).

9. Zhang Y, Gao G, Chan HLW, Dai J, Wang Y, Hao J. Piezo-Phototronic Effect-Induced Dual-Mode Light and Ultrasound Emissions from ZnS:Mn/PMN–PT Thin-Film Structures. *Advanced Materials* **24**, 1729-1735 (2012).

10. Zhuang Y, Xie R-J. Mechanoluminescence Rebrightening the Prospects of Stress Sensing: A Review. *Advanced Materials* **33**, 2005925 (2021).

11. Wang C*, et al.* Heartbeat-Sensing Mechanoluminescent Device Based on a Quantitative Relationship between Pressure and Emissive Intensity. *Matter* **2**, 181-193 (2020).

12. Qian X*, et al.* Printable Skin-Driven Mechanoluminescence Devices via Nanodoped Matrix Modification. *Advanced Materials* **30**, 1800291 (2018).

13. Wang C, Peng D, Pan C. Mechanoluminescence Materials for Advanced Artificial Skin. *Science Bulletin* **65**, 1147-1149 (2020).

14. Jang J*, et al.* Mechanoluminescent, Air-Dielectric MoS_2 Transistors as Active-Matrix Pressure Sensors for Wide Detection Ranges from Footsteps to Cellular Motions. *Nano Letters* **20**, 66-74 (2020).

15. Ding Y, So B, Cao J, Wondraczek L. Ultrasound-Induced Mechanoluminescence and Optical Thermometry Toward Stimulus-Responsive Materials with Simultaneous Trigger Response and Read-Out Functions. *Advanced Science* **9**, 2201631 (2022).

16. Hong G. Seeing the Sound. *Science* **369**, 638-638 (2020).

17. Wong M-C, Chen L, Tsang M-K, Zhang Y, Hao J. Magnetic-Induced Luminescence from Flexible Composite Laminates by Coupling Magnetic Field to Piezophotonic Effect. *Advanced Materials* **27**, 4488-4495 (2015).

18. Wong M-C, Chen L, Bai G, Huang L-B, Hao J. Temporal and Remote Tuning of Piezophotonic-Effect-Induced Luminescence and Color Gamut via Modulating Magnetic Field. *Advanced Materials* **29**, 1701945 (2017).

19. Chandra BP, Chandra VK, Jha P. Microscopic Theory of Elastico-Mechanoluminescent Smart Materials. *Applied Physics Letters* **104**, 031102 (2014).

20. Mukhina MV, Tresback J, Ondry JC, Akey A, Alivisatos AP, Kleckner N. Single-Particle Studies Reveal a Nanoscale Mechanism for Elastic, Bright, and Repeatable ZnS:Mn Mechanoluminescence in a Low-Pressure Regime. *ACS Nano* **15**, 4115-4133 (2021).

21. Sohn K-S, Timilsina S, Singh SP, Choi T, Kim JS. Mechanically Driven Luminescence in a ZnS:Cu-PDMS Composite. *APL Materials* **4**, 106102 (2016).

22. Wei XY*, et al.* Dynamic Triboelectrification-Induced Electroluminescence and its Use in Visualized Sensing. *Advanced Materials* **28**, 6656-6664 (2016).

23. Yang X*, et al.* Effective Repeatable Mechanoluminescence in Heterostructured $Li_{1-x}Na_xNbO_3$: Pr^{3+}. *Small* **17**, 2103441 (2021).

24. Qasem A, Xiong P, Ma Z, Peng M, Yang Z. Recent Advances in Mechanoluminescence of Doped Zinc Sulfides. *Laser & Photonics Reviews* **15**, 2100276 (2021).

25. Chen Y*, et al.* Addressable and Color-Tunable Piezophotonic Light-Emitting Stripes. *Advanced Materials* **29**, 1605165 (2017).

26. Kamran MA*, et al.* Large Tunable Luminescence by Mn(ii) Aggregates in Mn-Doped ZnS Nanobelts. *Journal of Materials Chemistry C* **5**, 8749-8757 (2017).

27. Thong DD, Heimbrodt W, Hommel D, Goede O. Optical Study of ZnS:Mn Thin Films with High Mn Concentrations. *physica status solidi (a)* **81**, 695-700 (1984).

28. De Visschere P*, et al.* Analysis of the Luminescent Decay of ZnS:Mn Electroluminescent Thin Films. *Journal of Luminescence* **65**, 211-219 (1995).

29. Vink AP, de Bruin MA, Roke S, Peijzel PS, Meijerink A. Luminescence of Exchange Coupled Pairs of Transition Metal Ions. *Journal of The Electrochemical Society* **148**, E313 (2001).

30. Song E*, et al.* Mn^{2+}-Activated Dual-Wavelength Emitting Materials Toward Wearable Optical Fibre Temperature Sensor. *Nature Communications* **13**, 2166 (2022).

31. Era K, Shionoya S, Washizawa Y. Mechanism of Broad-Band Luminescences in ZnS Phosphors—I. Spectrum Shift During Decay and with Excitation Intensity. *Journal of Physics and Chemistry of Solids* **29**, 1827-1841 (1968).

32. Wang X*, et al.* Dynamic Pressure Mapping of Personalized Handwriting by a Flexible Sensor Matrix Based on the Mechanoluminescence Process. *Advanced Materials* **27**, 2324-2331 (2015).

33. Lakes R. *Viscoelastic Materials*. Cambridge University Press (2009).

34. Feng A, Smet PF. A Review of Mechanoluminescence in Inorganic Solids: Compounds, Mechanisms, Models and Applications. *Materials* **11**, 484 (2018).

35. Era K, Shionoya S, Wasfflzawa Y, Ohmatsu H. Mechanism of Broad-Band Luminescences in ZnS Phosphors—II. Characteristics of Pair Emission Type Luminescences. *Journal of Physics and Chemistry of Solids* **29**, 1843-1857 (1968).

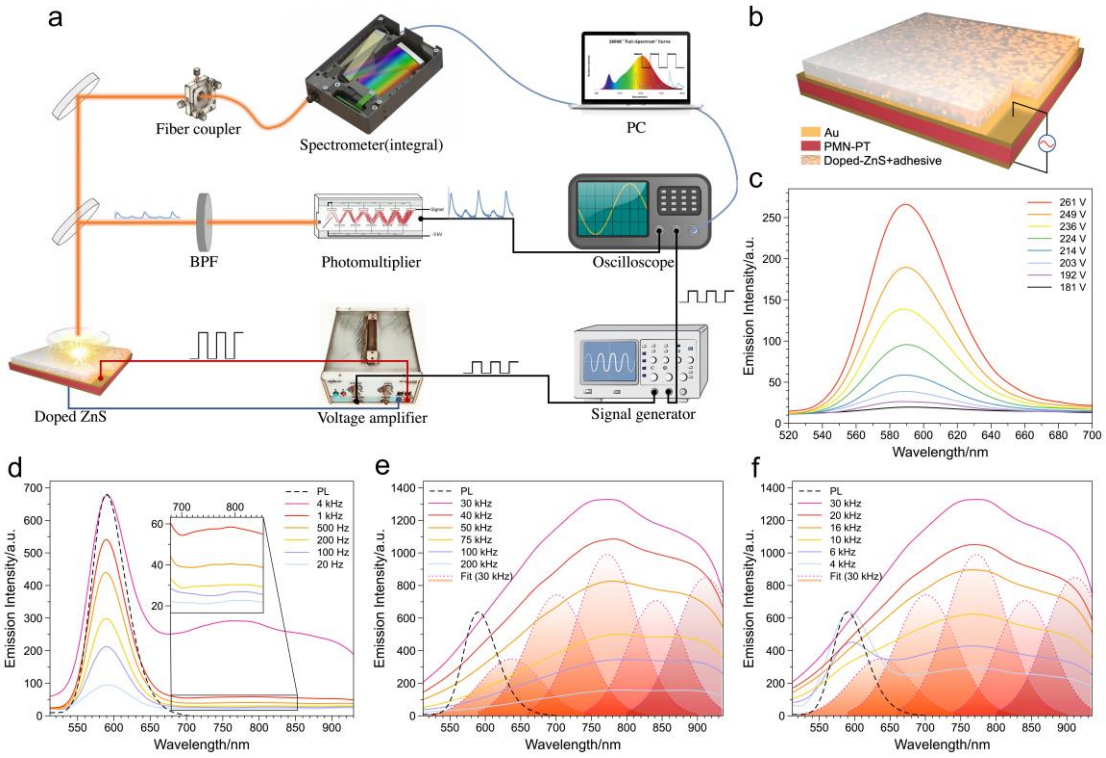

Figure 1. Amplitude-dependent and frequency-dependent EML spectra of ZnS:Mn composite. a) Sketch of steady state and transient state EML measurement architecture. b) Schematic of the doped ZnS composite integrated with PMN-PT substrate. c) EML spectra of ZnS:Mn composite obtained through the use of different voltage amplitudes, under fixed excitation frequency of 200 Hz. d-f) Characterization of EML of ZnS:Mn composite with different excitation frequency regions. 20 Hz – 4000 Hz (d), 2 kHz – 30 kHz (e), 30 kHz – 200 kHz (f). Five decomposed Gaussian components center at 636, 701, 772, 842 and 911 nm, respectively. These measurements were performed under rectangular wave voltage with

fixed strength of 200 V.

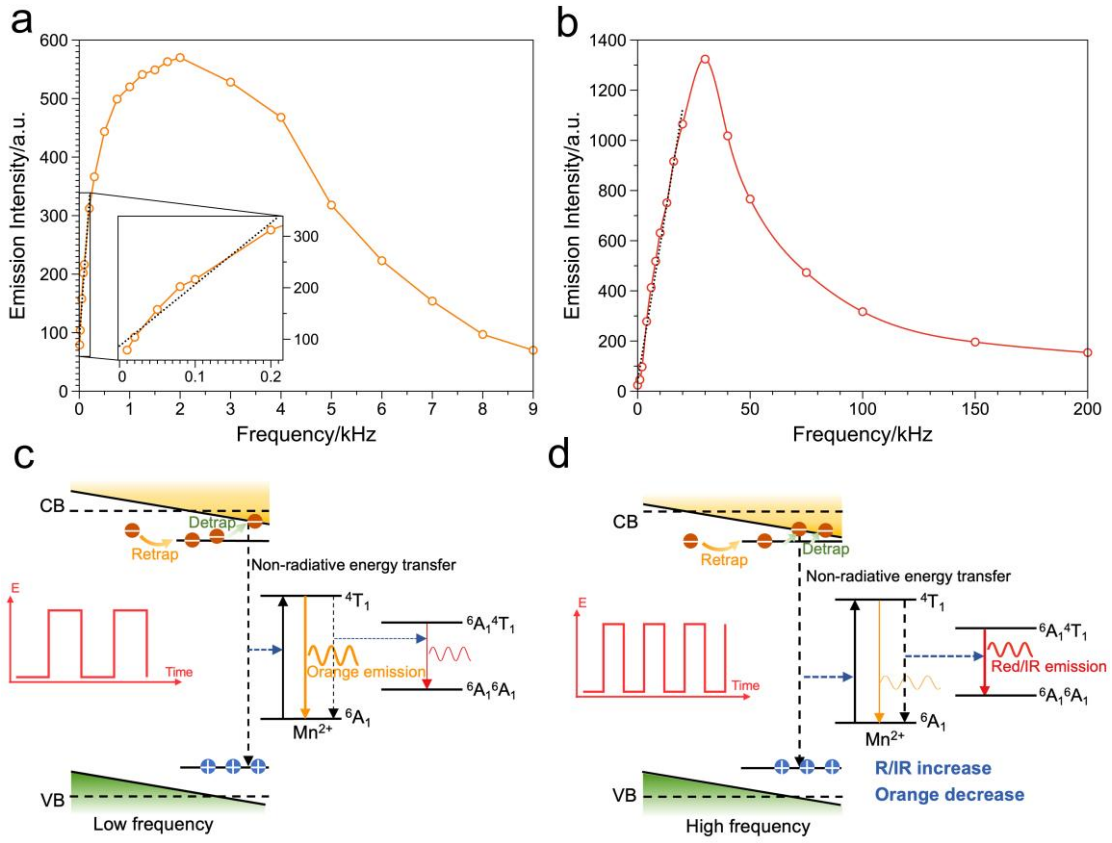

Figure 2. Frequency response of EML intensity of ZnS:Mn and proposed mechanism. a) Dependence of orange emission on the frequency of the rectangular wave voltage. b) Dependence of NIR emission on the frequency of the rectangular wave voltage. c, d) Schematic illustration of piezoelectricity-induced detrapping model for ZnS:Mn. Under low excitation frequency, EML of ZnS:Mn mainly origins from Mn^{2+} ion (c). Further increasing excitation frequency promotes the energy transfer from excited Mn^{2+} ions to the $(Mn)_n$ clusters, leading to the appearance and enhancement of NIR emission (d).

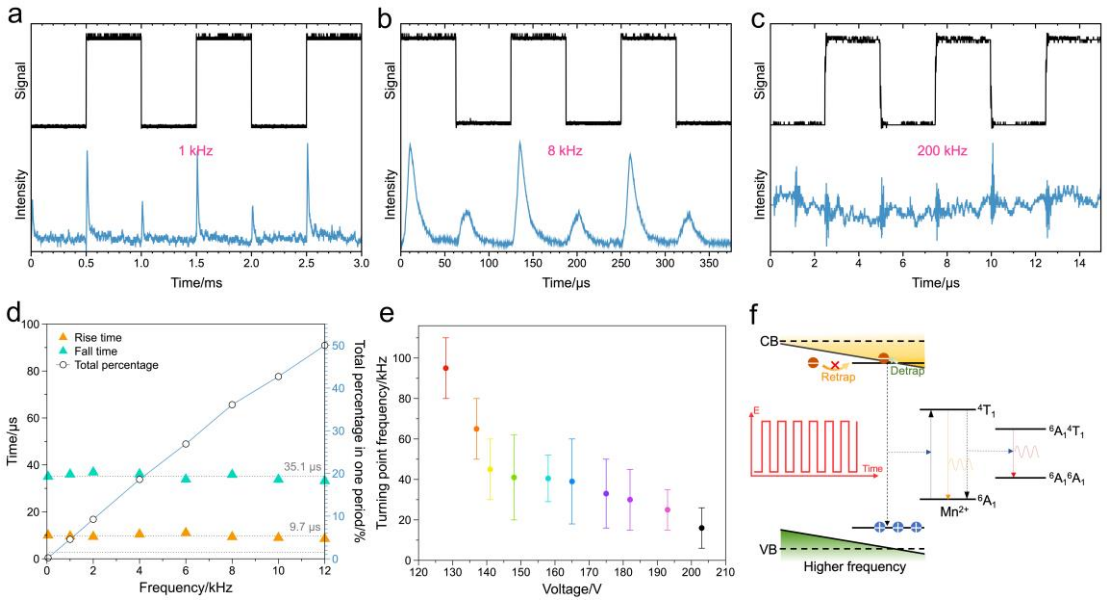

Figure 3. Characteristics and analysis of time-resolved EML of ZnS:Mn. a-c) Time-resolved EML of ZnS:Mn composite plotted in responding to the rectangular wave voltages of different frequencies. 1 kHz (a), 8 kHz (b), 200 kHz (c). d) Rise and fall time of EML emission as a function of frequency of the rectangular wave voltage. e) Turning point frequency of NIR emission versus the amplitude of the rectangular wave voltage. f) Schematic illustrating the model of high-frequency excitation induced EML quenching in ZnS:Mn. EML saturation and quenching of ZnS:Mn arise from the retrapping rate cannot keep pace with the excitation frequency.

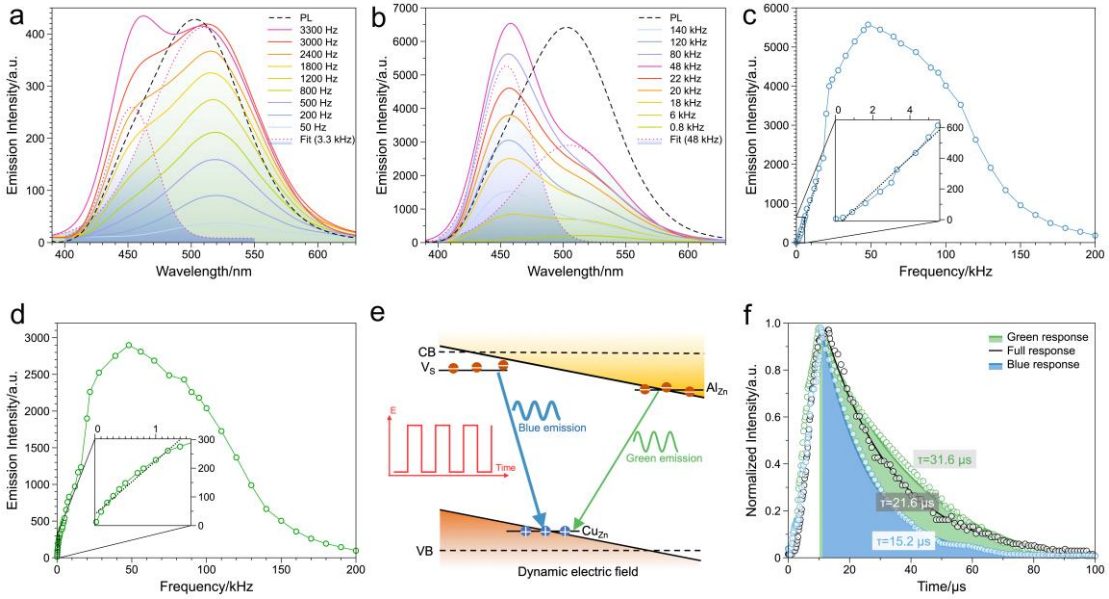

Figure 4. Frequency response of EML intensity of ZnS:Cu, Al and proposed mechanism. a, b) EML spectra of ZnS:Cu, Al with increasing the frequency of the rectangular wave voltage. 50 Hz – 3300 Hz (a), 0.8 kHz – 140 kHz (b). c, d) Dependence of EML intensity of ZnS:Cu, Al on the frequency of the rectangular wave voltage. Blue emission (c), Green emission (d). e) Schematic illustration of the trap-controlled donor-acceptor pair emission mechanism for ZnS:Cu, Al. Blue and green emission bands origin from the electron-hole recombination of donor-acceptor V_s - Cu_{Zn} and Al_{Zn} - Cu_{Zn} pairs, respectively. Upon high-frequency excitation, green EML emission from Al_{Zn} - Cu_{Zn} pairs is susceptible to saturation. f) EML decay curves of blue and green emissions.

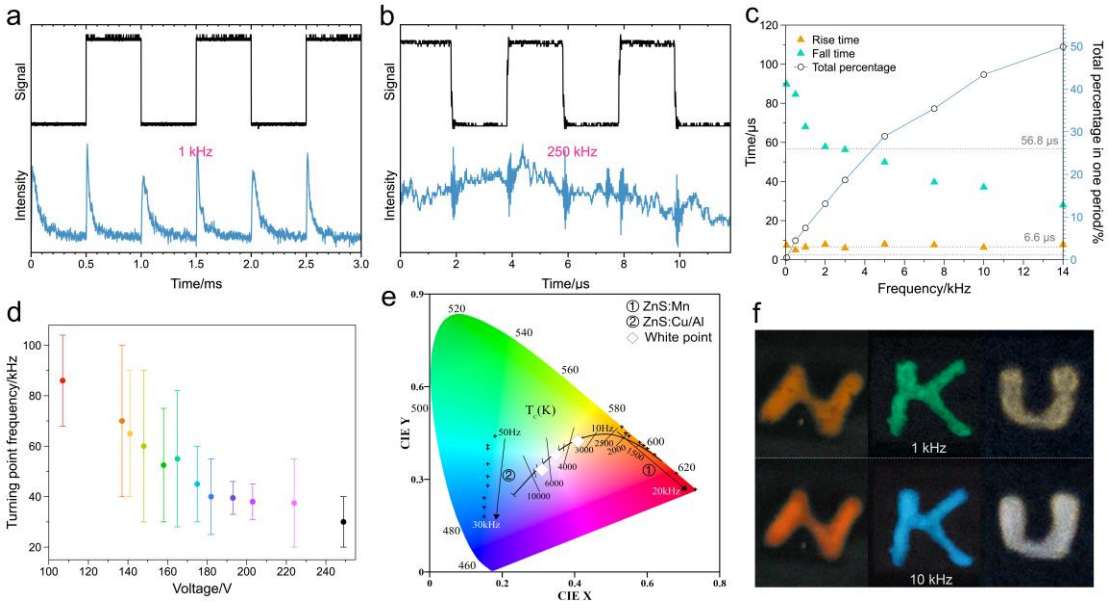

Figure 5. Characteristics and analysis of time-resolved EML of ZnS:Cu, Al. a, b) Time-resolved EML of ZnS:Mn composite plotted in responding to the rectangular wave voltages of different frequencies. 1 kHz (a), 250 kHz (b). c) Rise and fall times of EML emission as a function of frequency of the rectangular wave voltage. d) Turning point frequency of NIR emission versus the amplitude of the rectangular wave voltage. e) The CIE coordinates showing the color tuning with the frequency changing. f) Photographs showing the color variation of the letters made of EML phosphors by turning the excitation frequency.

The table of contents entry should be 50−60 words long and should be written in the present tense and impersonal style (i.e., avoid we). The text should be different from the abstract text.

Temporal mechanoluminscence (ML) behaviors are studied in unexplored high-frequency range via piezoelectric actuation. Time-resolved ML of representative phosphors ZnS:Mn and ZnS:Cu, Al shows unrevealed frequency-dependent saturation and quenching. Proof-of-concept devices demonstrate red-green-blue full color and white-light emissions. These findings offer insight into the photophysics nature of ML and broaden physical modulation manner by locally adjusting the excitation frequency.

Keyword:(mechanoluminescence, piezoelectricity, self-recovery, tunable luminescence, cluster)

Tianhong Zhou, Haisheng Chen, Jiaxing Guo, Yanan Zhao, Xiaona Du, Qingyi Zhang, Wenwen Chen, Taiyu Bian, Zhi Zhang, Jiaying Shen, Weiwei Liu, Yang Zhang,* Zhenping Wu,* Jianhua Hao*

Unrevealing temporal mechanoluminescence behaviors at high frequency via piezoelectric actuation

ToC figure ((Please choose one size: 55 mm broad ×50 mm high **or**110 mm broad ×20 mm high. Please do not use any other dimensions))